Article

Visible Light-Driven Photocatalytic Degradation of Ciprofloxacin, Ampicillin and Erythromycin by Zinc Ferrite Immobilized on Chitosan

Nehad Ahmed Hassan Mohamed [1], Rehab Nabil Shamma [2,*] , Sherien Elagroudy [1,3] and Adewale Adewuyi [4,5,*]

[1] Public Works Department, Faculty of Engineering, Ain Shams University, Cairo 11535, Egypt
[2] Department of Pharmaceutics and Industrial Pharmacy, Faculty of Pharmacy, Cairo University, Cairo 11561, Egypt
[3] Egypt Solid Waste Management Center of Excellence, Ain Shams University, Cairo 11535, Egypt
[4] Department of Chemical Sciences, Faculty of Natural Sciences, Redeemer's University, Ede 230, Osun State, Nigeria
[5] Yusuf Hamied Department of Chemistry, University of Cambridge, Lensfield Road, Cambridge CB2 1EW, UK
[*] Correspondence: rehab.shamma@pharma.cu.edu.eg (R.N.S.); walexy62@yahoo.com (A.A.); Tel.: +20-111-930-1245 (R.N.S.); +2348035826679 (A.A.)

Abstract: This study investigated the synthesis of zinc ferrite immobilized on chitosan ($ZnFe_2O_4$@Chitosan) and its application in the photodegradation of ciprofloxacin (CIP), ampicillin (AMP) and erythromycin (ERY) in aqueous solution. Results from Fourier transform infrared spectroscopy (FTIR) revealed peaks suggesting its synthesis, while signals from X-ray diffraction (XRD) showed diffraction patterns confirming the synthesis of $ZnFe_2O_4$@Chitosan with a crystallite size of 35.14 nm. Scanning electron microscopy (SEM) revealed a homogeneous morphology with a surface area of 12.96 m^2 g^{-1} from the Brunauer–Emmett–Teller (BET) analysis. The vibrating sample magnetometry (VSM) result revealed a saturation magnetization of 2.38 emu g^{-1}. The photodegradation study of CIP, AMP and ERY showed that both photodegradation and adsorption were taking place at the same time with the percentage degradation efficiency in the order CIP (99.80 ± 0.20%) > AMP (94.50 ± 0.10%) > ERY (83.20 ± 0.20%). $ZnFe_2O_4$@Chitosan exhibited high stability with capacity > 90% even at the 15th regeneration cycle, suggesting a viable economic value of $ZnFe_2O_4$@Chitosan.

Keywords: adsorption; antibiotics; catalysis; ferrite; photodegradation

1. Introduction

Contamination of natural sources of drinking water by antibiotics is a global concern [1]. The contamination is on the rise because of the unregulated use of antibiotics in some nations of the world [2]. The ease of purchasing antibiotics without medical prescription in some countries has encouraged self-medication, resulting in the excessive use of antibiotics. The excessive use of antibiotics is one of the causes of their presence in environmental natural water-like surface and underground water systems. These antibiotics may become persistent in the environment or may decompose to form products that are toxic to humans and the environment. Some of the decomposition products can cause serious health challenges like cancer. Apart from this, the presence of antibiotics in the environmental natural water system has led to far more serious consequences like the emergence of drug-resistant strains of pathogenic organisms [3], which, in turn, hampered the efficacies of well-known antibiotics. Unfortunately, previously efficient antibiotics are now losing efficacy. It is important that these antibiotics are removed from water in order to avoid the challenges associated with their presence in natural sources of drinking water.

Many antibiotics have been detected in water [4,5], including ciprofloxacin (CIP), ampicillin (AMP) and erythromycin (ERY) reported in surface water as contaminants [6–9].

Their presence in water is of serious concern, although efforts have been made to remove them from water, but most of these efforts have shortcomings, like incomplete removal or being expensive. It is important to develop a process that can overcome such shortcomings with an affordable and sustainable approach. Photocatalysis is a green approach which has shown exceptional performance in the degradation of organic pollutants in water [10–12]. Photocatalysis has the potential of overcoming these shortcomings with the capacity for complete degradation of antibiotics in water [13]. Zinc oxide (ZnO) is an example of a photocatalyst that can be used in photocatalysis for the photocatalytic degradation of antibiotics. Unfortunately, ZnO is limited in its photocatalytic application, because it is photoactive in UV light due to its large bandgap energy.

Previous studies have reported the use of ZnO particles for the degradation of amoxicillin, CIP, AMP and cloxacillin under UV light irradiation in aqueous solutions [14]. The study revealed a degradation efficiency of approximately 50% for CIP, creating the need for improvement. ZnO is active under UV light irradiation, which increases the process cost since there is a need to get a UV light source, unlike in the case of materials which are visible-light sensitive. A similar observation was also recorded recently using ZnO-functionalized fly-ash-based zeolite for the degradation of CIP which exhibited complete degradation [15]; despite the complete degradation, provision of UV light sources is an additional cost which eventually increases process cost. Developing ZnO into materials that are visible-light sensitive will go a long way in helping to reduce process cost. One of the ways of achieving this will be to incorporate ZnO into other particles, which reduces its bandgap energy. A good example of this is zinc ferrite ($ZnFe_2O_4$). Ferrites are useful in this regard because of their relatively narrow bandgap of approximately 2.0 eV, which makes it suitable for photocatalysis in the visible-light region.

Spinel ferrites were recently reported for the degradation of tetracycline hydrochloride [16]. Moreover, magnesium ferrite ($MgFe_2O_4$) and manganese ferrite ($Mn_xFe_{3-x}O_4$) have shown similar capacities against tetracycline [17] and sulfamethoxazole [18], respectively. Furthermore, high performance has been reported from the synergistic activity of $MnFe_2O_4$ and molybdenum disulfide (MoS) for the degradation of tetracycline [19]. Photocatalytic degradation of antibiotics by ferrite has proved to be a good solution for the treatment of antibiotic-contaminated water due to its soft magnetic properties, high catalytic activities and ease of recycling through magnetic separation [20]. However, a recent study revealed that the performance of a photocatalyst can be enhanced via a simple modification process. The current study proposes the modification of $ZnFe_2O_4$ by organic molecule such as chitosan. The use of chitosan will help stabilize the particles of $ZnFe_2O_4$ by reducing aggregation and helping to promote the recovery of $ZnFe_2O_4$ particles from solution. A previous study has shown that the efficiency of modified photocatalysts may be attributed to high light absorption, formation of step scheme heterojunction and interfacial charge separation. Being a polysaccharide, chitosan contains random distribution of β-(1–4)-linked D-glucosamine and N-acetyl-D-glucosamine. It is either neutral or negatively charged in acidic medium, which allows it to form electrostatic complexes or multilayer structure. Its nontoxicity, biocompatibility and biodegradability make it suitable for various applications such as in water treatment.

This study aimed at investigating the preparation of $ZnFe_2O_4$ via coprecipitation and its immobilization on chitosan to further improve on its separation from aqueous solution when used as a photocatalyst for the photodegradation of antibiotics. $ZnFe_2O_4$@Chitosan was proposed as a photocatalyst for the degradation of CIP, AMP and ERY in aqueous solution. Therefore, this study was aimed at the photodegradation of CIP, AMP and ERY under visible-light irradiation using $ZnFe_2O_4$@Chitosan.

2. Materials and Methods

2.1. Materials

Zinc chloride hexahydrate ($ZnCl_2.6H_2O$), ferric chloride hexahydrate ($FeCl_3.6H_2O$), chitosan, acetic acid, NaOH, C_2H_5OH, HCl, oleic acid, ciprofloxacin (CIP), ampicillin

(AMP), erythromycin (ERY), isopropyl alcohol (IPA), ammonium oxalate (AO), chloroform (CH), and all other chemicals used were purchased from the Aldrich Chemical Co., Gillingham, UK.

2.2. Synthesis of $ZnFe_2O_4$ Particles

To prepare $ZnFe_2O_4$ particles, mixtures of $FeCl_3.6H_2O$ (0.4 M) and $ZnCl_2.6H_2O$ (0.2M) were continuously stirred for 60 min, after which oleic acid (15 mL) was added as a capping agent. The mixture was maintained at a temperature of 80 °C and a pH range of 10–12 by dropwise addition of NaOH (2 M) until the appearance of precipitate while stirring for 2 h. The mixture was cooled to room temperature, filtered, and washed severally with water and ethanol. The residue obtained was oven-dried at 105 °C for 12 h and transferred to the furnace at 550 °C for 18 h.

2.3. Synthesis of $ZnFe_2O_4$@Chitosan Particles

To prepare $ZnFe_2O_4$@Chitosan, chitosan (1 g) was dissolved in acetic acid (50 mL, 2% v/v) and sonicated for 60 min. $ZnFe_2O_4$ (2 g) was added to the solution and stirred for 60 min. While maintaining room temperature, 30 mL of NaOH (1 M) were added and stirred for 40 min to form precipitates. The $ZnFe_2O_4$@Chitosan formed was filtered and washed severally with deionized water. The residue obtained was oven-dried at 40 °C for 12 h.

2.4. Characterization of $ZnFe_2O_4$@Chitosan Particles

The functional groups in $ZnFe_2O_4$@Chitosan were determined using FTIR (Agilent Technologies); spectrum was recorded in the range of 400–4500 cm^{-1}. The BET surface area was determined by N_2 gas adsorption using Nova 3200 quanta chrome. TG analysis was carried out using a Mettler thermogravimetric analyzer (SDT Q600 V20.9 Build 20). The X-ray diffraction pattern was measured in 2θ ranging from 5 to 90° using an X-ray diffractometer (Philip XRD-1390 PW model) with filtered Cu Kβ radiation operated at 40 kV and 40 mA. The SEM image was recorded using SEM JSM-T25 (JOEL Co., Japan), while elemental composition was estimated on EDS. VSM was carried out on a magnetometer and UV-visible absorption spectra were recorded on a UV-visible spectrophotometer (UV-vis: Cary 60).

2.5. Photocatalytic Degradation of CIP, AMP and ERY by $ZnFe_2O_4$@Chitosan

The photodegradation study was carried out under visible light using a low-cost solar simulator (LSO1O6, 150 W Xe light source) with a filter holder and 90° beam turner. The degradation was achieved by contacting 100 mL of either CIP, AMP or ERY at a concentration of 5.00 mg L^{-1} with 0.1 g of $ZnFe_2O_4$@Chitosan particle in a 150 mL beaker for 180 min while stirring gently at 80 rpm under the simulated visible-light irradiation, ensuring a distance of 20 cm between the UV lamp and the test solution. Samples were withdrawn at different intervals to monitor the degradation rate. The concentrations of CIP (λ_{max} = 271 nm), AMP (λ_{max} = 420 nm) and ERY (λ_{max} = 285 nm) were measured using a UV-visible spectrophotometer (Perkin Elmer, Lambda 750 spectrometer). The effect of the $ZnFe_2O_4$@Chitosan weight on degradation was checked by varying the weight of $ZnFe_2O_4$@Chitosan from 0.1 to 0.5 g, while the effect of concentration of CIP, AMP or ERY on degradation capacity was evaluated by varying the concentration from 1.00 to 5.00 mg L^{-1} (CIP, AMP or ERY), and the effect of pH was determined by varying the pH solution from 2 to 10. The experiment was repeated in the dark to establish the adsorption–desorption equilibrium. All the experiments were repeated three times and values were presented as mean value. The degradation efficiency was calculated as:

$$Degradation\ Efficiency\ (\%) = 100\ x\ (1 - \frac{C_t}{C_o}) \tag{1}$$

where C_o is the initial concentration of CIP, AMP or ERY, and C_t is the concentration of CIP, AMP or ERY at time t. The adsorption capacity (q_t) and the percentage removal (% removal) for the adsorption–desorption equilibrium experiment in the dark was calculated as:

$$q_t = \frac{(C_o - C_t)V}{m} \tag{2}$$

$$\% \, removal = \frac{(C_o - Ct)}{Co} \, X \, 100 \tag{3}$$

Equation (4) was obtained by combining Equations (2) and (3)

$$q_t = \frac{(\% \, removal \, X \, C_o \, X \, V)}{100 \, X \, m} \tag{4}$$

where C_o (mg L^{-1}) is the initial concentration of CIP, AMP or ERY, C_t (mg L^{-1}) is the concentration of CIP, AMP or ERY at time t; m is the weight (g) of ZnFe$_2$O$_4$@Chitosan used, V represents the volume in litres (L) and q_t (mg g^{-1}) is the adsorption capacity.

2.6. Evaluation of Reactive Oxygen Species Scavenging Capacity

In order to understand the mechanism of operation of ZnFe$_2$O$_4$@Chitosan, the role of reactive oxygen species (ROS) in the photodegradation of CIP, AMP and ERY was investigated using isopropyl alcohol (IPA) as a hydroxyl radical (OH·) scavenger, ammonium oxalate (AO) as a scavenger for hole (h$^+$) and the scavenger for superoxide ion radical ($\cdot$O$_2^-$) being chloroform (CH). The scavengers were separately introduced into the photodegradation process as a concentration of 1 mM. The process conditions (ZnFe$_2$O$_4$@Chitosan weight, concentration of CIP, AMP or ERY, photodegradation time, and pH) for photodegradation with and without scavengers was kept constant.

2.7. Re-Useability and Stability of ZnFe$_2$O$_4$@Chitosan

To determine re-useability, the ZnFe$_2$O$_4$@Chitosan was recovered after the degradation time, washed with solvents (deionized water, 0.1 M HCl, ethanol or a mixture of ethanol and 0.1 M HCl (3:2)) and dried in the oven at 80 °C for 5 h before it was reused for the photodegradation process. The treated aqueous solution was analyzed to check for the leaching of ZnFe$_2$O$_4$ into solution using inductively coupled plasma–optical emission spectroscopy (ICP–OES). The ICP–OES analysis was carried out at the end of each treatment cycle with ZnFe$_2$O$_4$@Chitosan. The photostability of the ZnFe$_2$O$_4$@Chitosan for the photodegradation of CIP, AMP and ERY was evaluated in fifteen (15) successive cycles of operation.

3. Results and Discussion

3.1. Synthesis and Characterization of ZnFe$_2$O$_4$@Chitosan

The FTIR spectrum of ZnFe$_2$O$_4$@Chitosan revealed the functional groups it contained, as shown in Figure 1a. The spectrum revealed a peak at 3420 cm^{-1}, which was attributed to the O-H stretching, while the peak at 2892 cm^{-1} was assigned to the C-H stretching of alkane. The -NH$_3$C stretch was observed at 2352 cm^{-1}, while the signal corresponding to the C=O carbonyl stretch of amide was seen at 1612 cm^{-1}. The N-H and C-H bending appeared at 1584 and 1580 cm^{-1}, respectively. The peak at 1432 cm^{-1} was assigned to C-O stretch, while the anti-asymmetric stretching vibration of C-O-C appeared at 1027 cm^{-1}. The signals appearing at 593 and 387 cm^{-1} correspond to the stretching frequencies of Zn-O and Fe-O, respectively. The BET surface area of ZnFe$_2$O$_4$@Chitosan is shown in Figure 1b, which revealed a surface area of 12.96 m^2 g^{-1}, total pore volume (at P/P$_o$ = 0.900) of 0.109 cm^{3}g^{-1} and a mean pore diameter of 33.71 nm. The BET isotherm exhibited by ZnFe$_2$O$_4$@Chitosan is of type II, which suggests unrestricted monolayer–multilayer adsorption that is common to mesoporous adsorbents [21]. The XRD diffraction (Figure 1c) showed the most intense peak at 2θ = 35.61° with a plane spacing corresponding to

(311), which is the plane previously reported for $ZnFe_2O_4$ particles [22] with other planes corresponding to (110), (111), (134), (220), (222), (400), (422), (511), (440), (620), (533), (444), (642), (731) and (800), as seen in the pattern [22,23]. Equation (5) shows an expression from which the crystallite size of $ZnFe_2O_4$@Chitosan may be calculated considering its X-ray line broadening from the reflections of (311) and Debye–Scherrer's formula [24]:

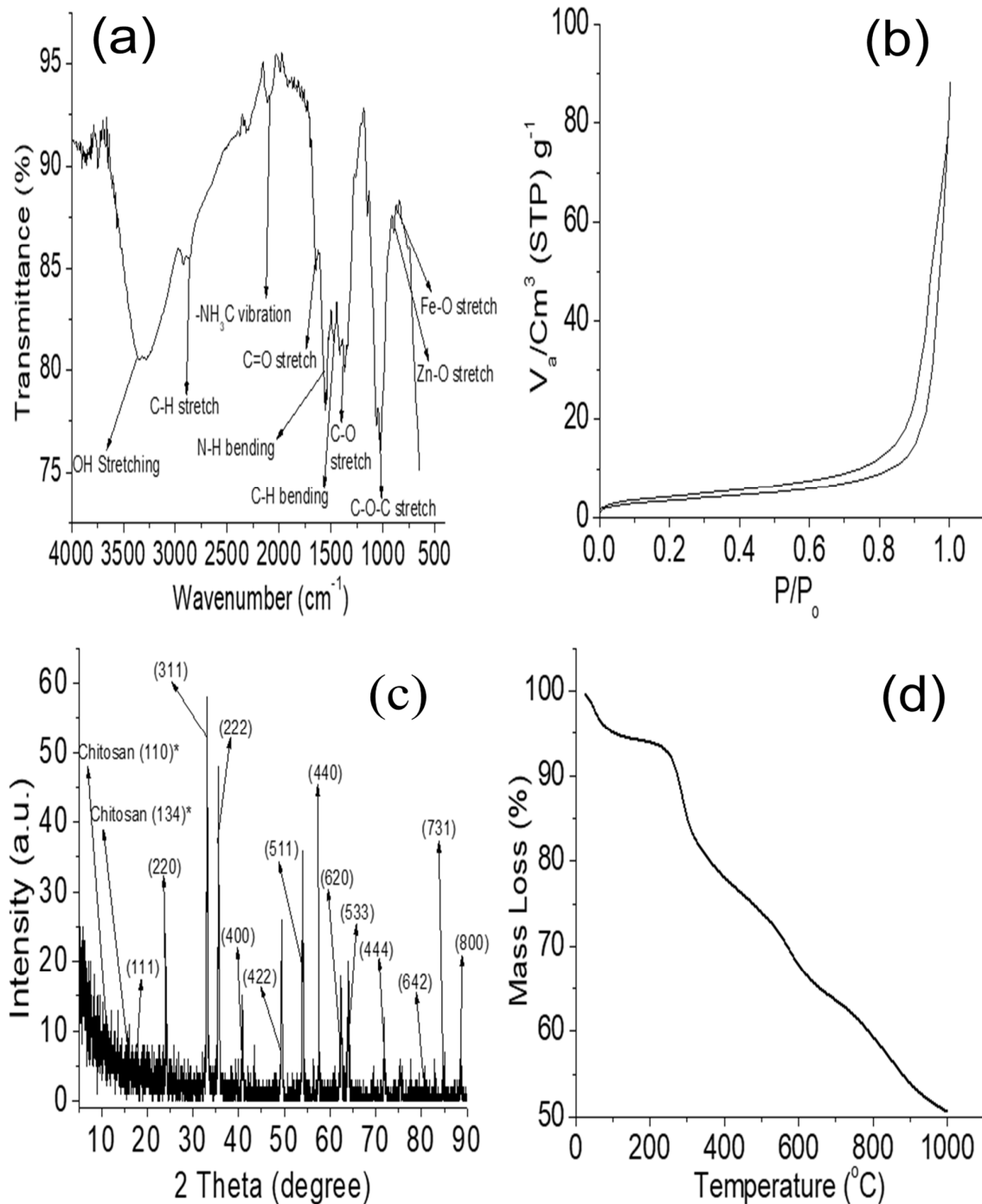$$D = \frac{K\lambda}{\beta \, Cos\theta} \tag{5}$$

Figure 1. FTIR (**a**), BET (**b**), XRD (**c**) and TGA analysis (**d**) of $ZnFe_2O_4$@Chitosan.

From Equation (5), D is the average crystallite size of $ZnFe_2O_4$@Chitosan, K represents a constant taken as 0.89. λ is the X-ray wavelength (1.5406 Å), while β and θ are the full width of diffraction line at half of the maximum intensity (FWHM) and Bragg's angle (at peak (311)), respectively [25]. The crystallite size for $ZnFe_2O_4$@Chitosan was found to be 35.14 nm. The crystallite size is important in understanding its diffusion properties. Apparently, this can be expressed as [26,27]:

$$Ʈ = r^2 л^2 D \tag{6}$$

where Ʈ is the average diffusion time of charge carriers from bulk solution to the surface of $ZnFe_2O_4$@Chitosan, and D represents the diffusion coefficient of the charges. According to the expression (Equation (6)), the larger the size of a catalyst, the longer the diffusion time, which means the more susceptible it is to aggregation (recombination effect). Such recombination leads to decreased catalytic property [27,28]. It is important that the crystallite size is small. The crystallite size of $ZnFe_2O_4$@Chitosan falls withing the range of previously reported sizes (37 to 45 nm) for spinel ferrite [29], suggesting a good catalyst functional size for $ZnFe_2O_4$@Chitosan.

The thermal degradation is shown in Figure 1d, which showed three major losses. The first loss at range 0–180 °C is about 5.58%, which was attributed to a loss of volatile and adsorbed water molecules. This is followed by a second major loss at range 210–415 °C, which is 17.41% of total mass and was attributed to the decomposition of the chitosan structure with loss of H_2O, NH_3, CO, CO_2 and CH_3COOH, which was considered to be pyrrolic degradation of chitosan as previously reported [30,31]. Moreover, previous study has shown that the degradation of chitosan can take place by random breaking of the C-O-C skeletal bond [30–33], which was seen in the FTIR result (Figure 1a) at 1027 cm^{-1}. The third important loss in the range 415–1000 °C accounts for 26.30% loss of the total mass, which may be attributed to loss of CH_4 that was considered to have taken place via a dehydrogenation mechanism as previously reported [30,34,35].

The SEM micrograph is presented in Figure 2a, revealing district packs of particles on the surface of $ZnFe_2O_4$@Chitosan which may be seen to be homogeneous. The EDS result (Figure 2b) confirms the presence of carbon (c), oxygen (O), nitrogen (N), iron (Fe) and zinc (Zn) in the molecule of $ZnFe_2O_4$@Chitosan, while elemental surface mapping is shown in Figure 2c ($C_{1–5}$).

The magnetic property of $ZnFe_2O_4$@Chitosan was investigated using vibration sample magnetometry and the results are presented in Figure 2d with magnetic hysteresis loop, indicating that $ZnFe_2O_4$@Chitosan is magnetic. The saturation magnetization is found to be 2.38 emu g^{-1}, which is large enough for magnetic separation for practical applications. Previous study has reported a high saturation magnetization [22,36,37] for $ZnFe_2O_4$; however, the observed low saturation magnetization in $ZnFe_2O_4$@Chitosan compared to previous reports may be due to the immobilization of $ZnFe_2O_4$ on chitosan, which may have altered the inversion degree of $ZnFe_2O_4$.

The UV-visible spectrum is shown in Figure 3a, revealing absorbance in the visible region, which suggests that $ZnFe_2O_4$@Chitosan may have photocatalytic activity in the visible-light region. The optical bandgap was determined from the Tauc plot method, as shown in Figure 3b; this was determined as described for a transition-type semiconductor (Equation (7):

$$(\propto hv)^2 = A\left(hv - E_g\right) \tag{7}$$

where hv is the frequency of incident light, A represents the proportionality constant, E_g is the bandgap and α is the absorption coefficient. The bandgap for $ZnFe_2O_4$@Chitosan was found to be 2.98 eV, which further corroborates the fact that $ZnFe_2O_4$@Chitosan may be active for photodegradation within the visible-light region.

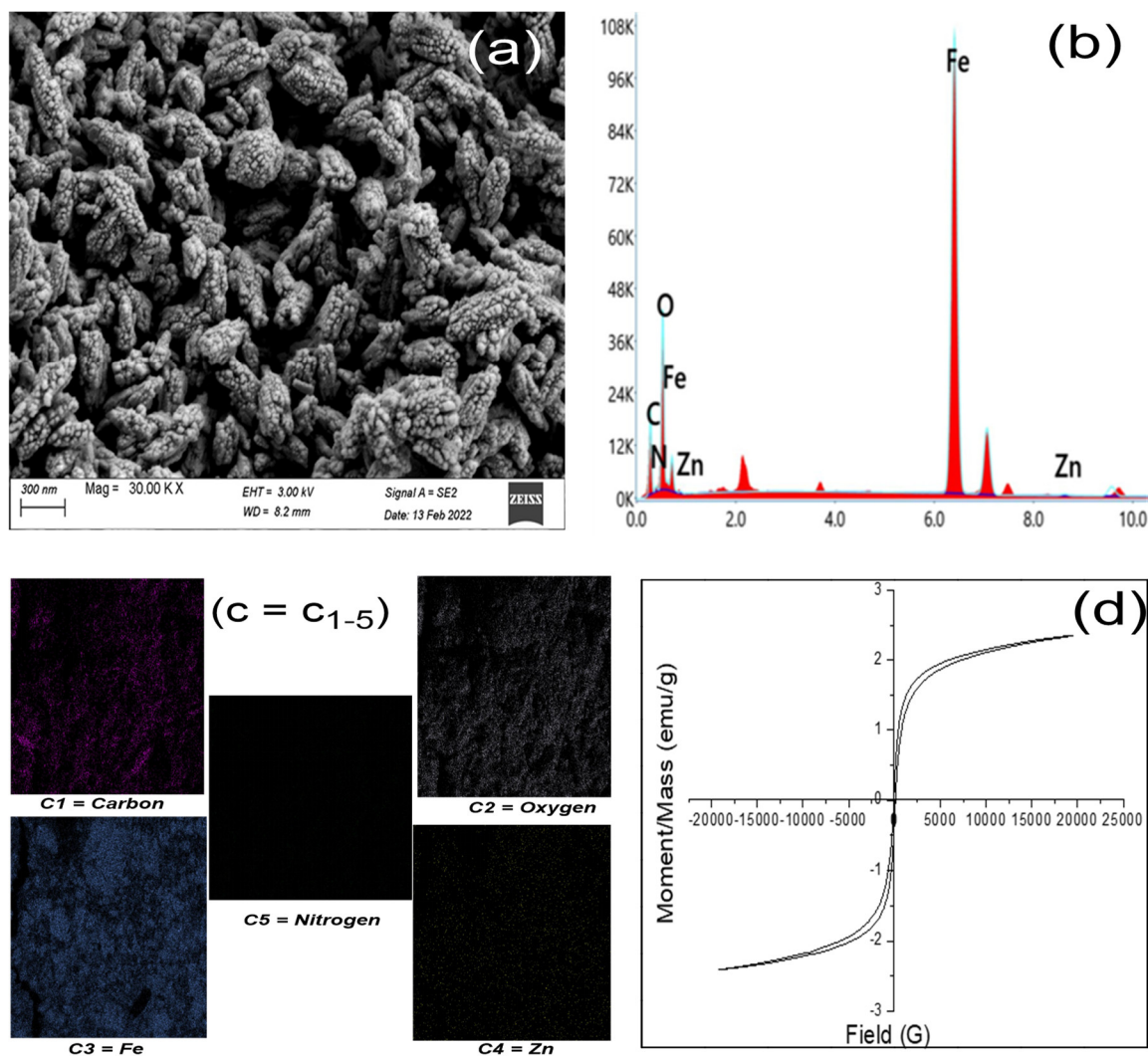**Figure 2.** SEM (**a**), EDS (**b**), surface mapping (**c**) and VSM analysis (**d**) of $ZnFe_2O_4$@Chitosan.

3.2. Photodegradation Study

The time-dependent degradation of CIP, AMP and ERY by $ZnFe_2O_4$@Chitosan at a concentration of 5.00 mg L^{-1} is presented in Figure 4a. The percentage degradation was in the following order of efficiency: CIP (99.80 ± 0.20%) > AMP (94.50 ± 0.10%) > ERY (83.20 ± 0.20%). The photodegradation reached equilibrium after 150 min of treatment. The degradation efficiency exhibited by $ZnFe_2O_4$@Chitosan towards the antibiotics might be molecular weight-dependent since the highest efficiency was found in CIP having the lowest molecular weight and the least efficiency found in ERY having the highest molecular weight. The molecular weight is in the increasing order of CIP (331.347 g mol^{-1}) < AMP (349.406 g mol^{-1}) < ERY (733.930 g mol^{-1}). The molecular structures of the antibiotics are shown in Figure 3c–e; the lower the molecular weight, the higher the degradation efficiency expressed by $ZnFe_2O_4$@Chitosan. The dark experiment revealed that adsorption was taking place at the same time with the photocatalytic degradation. Therefore, the adsorption capacities as well as the percentage removal with time are presented in Figure 4b–d. The adsorption capacity and percentage removal increased with time and reached equilibrium after 30 min of treatment. The adsorption capacity was 1.1 ± 0.05 mg g^{-1} in CIP, 0.6 ± 0.05 mg g^{-1} in AMP, and 1.6 ± 0.02 mg g^{-1} in ERY, while the percentage removals were 22 ± 0.05, 12 ± 0.05 and 32 ± 0.02% in CIP, AMP and ERY, respectively. The highest adsorption capacity and percentage removal was expressed towards ERY.
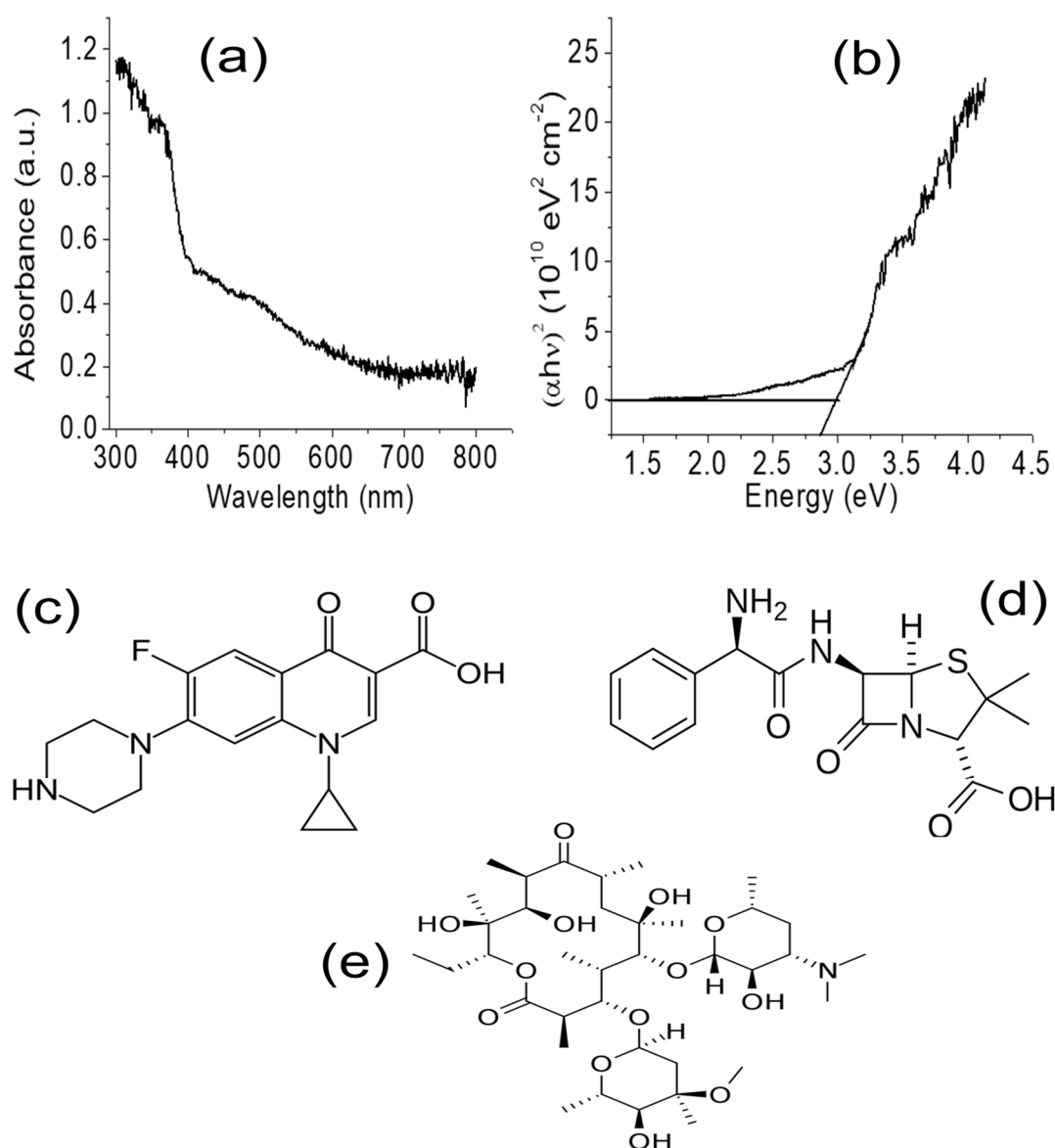
Figure 3. UV-visible absorbance spectra of ZnFe$_2$O$_4$@Chitosan (**a**), Tauc plot for ZnFe$_2$O$_4$@Chitosan (**b**), structure of CIP (**c**), structure of AMP (**d**) and structure of ERY (**e**).

3.3. Effect of Operational Parameters

The effect of concentration (1.00 to 5.00 mg L^{-1}) on degradation efficiency and percentage removal (dark experiment) are presented in Figure 5a,b, respectively. The degradation efficiency increased as concentration reduced from 5.00 to 1.00 mg L^{-1}, which may be due to the reduction in the amount of antibiotic species to be degraded. As these species reduce, ZnFe$_2$O$_4$@Chitosan had lesser work to execute, which resulted in an increase in efficiency. Moreover, when the concentration increases, more degradation products are produced that may occupy the active photodegradation site on ZnFe$_2$O$_4$@Chitosan. Therefore, since adsorption has been confirmed to be taking place from the dark experiment conducted, it becomes evident that, as adsorption takes place, there is the possibility of the photodegradation sites being populated with the adsorbed species as concentration increases, allowing more adsorbate to migrate to the photocatalysis sites on ZnFe$_2$O$_4$@Chitosan. This occurrence will reduce photon penetration or migration to the surface of ZnFe$_2$O$_4$@Chitosan to initiate photocatalytic activities. This incident is capable of reducing the formation of oxidants, which limits the interaction between generated holes and electrons in the conduc-

tion band. However, contrary to this, the percentage removal increased with an increase in concentration of the antibiotics, which may be due to the fact that, as the concentration of antibiotics in solution increased, more species were available to interact with the surface of $ZnFe_2O_4$@Chitosan for adsorption.
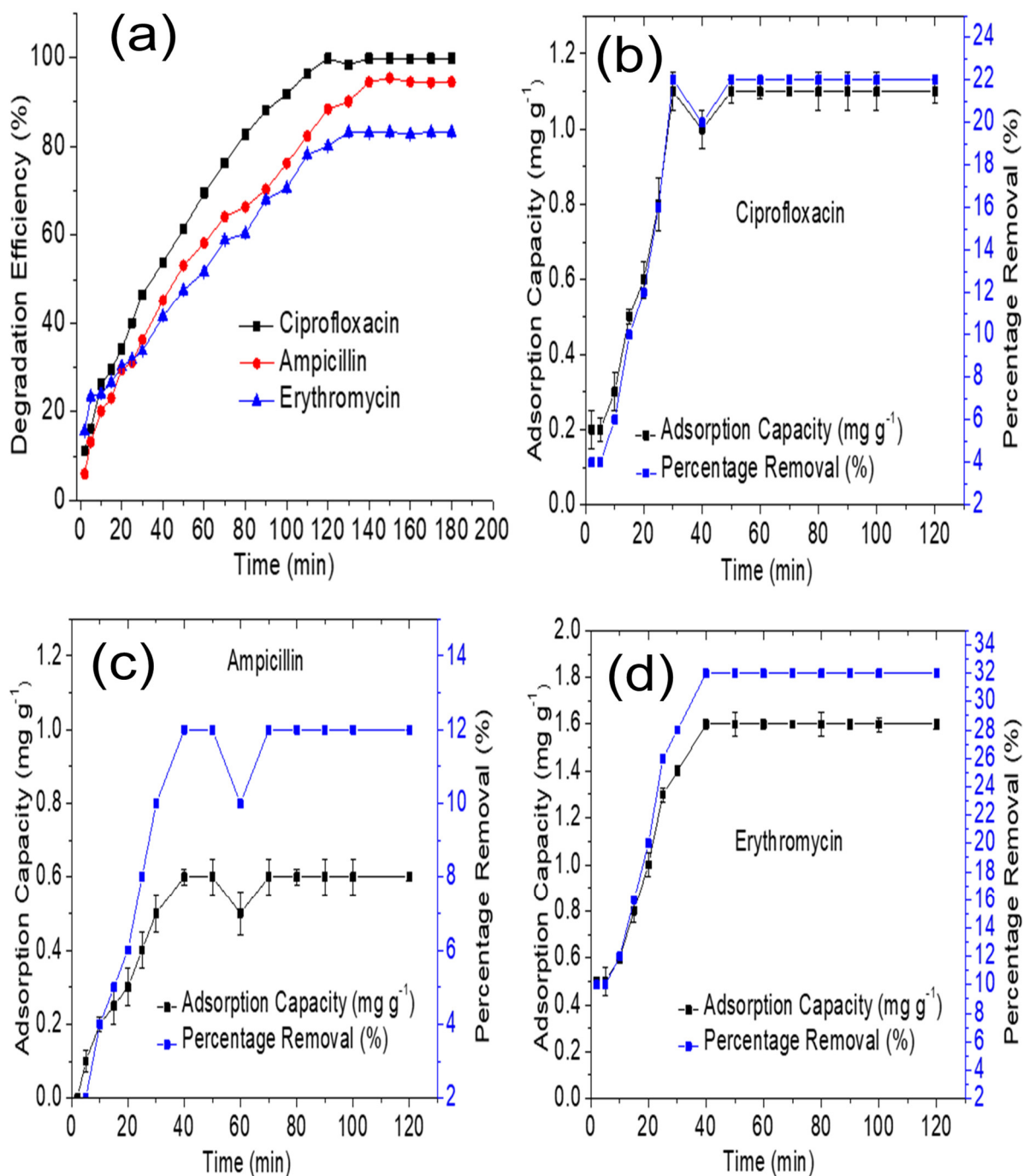

Figure 4. (**a**) = Time-dependent degradation efficiency for CIP, AMP and ERY at 5.00 mg L^{-1}, (**b**) = Adsorption capacity and percentage removal for CIP at 5.00 mg L^{-1} in the absence of visible light, (**c**) = Adsorption capacity and percentage removal for AMP at 5.00 mg L^{-1} in the absence of visible light and (**d**) = Adsorption capacity and percentage removal for ERY at 5.00 mg L^{-1} in the absence of visible light.
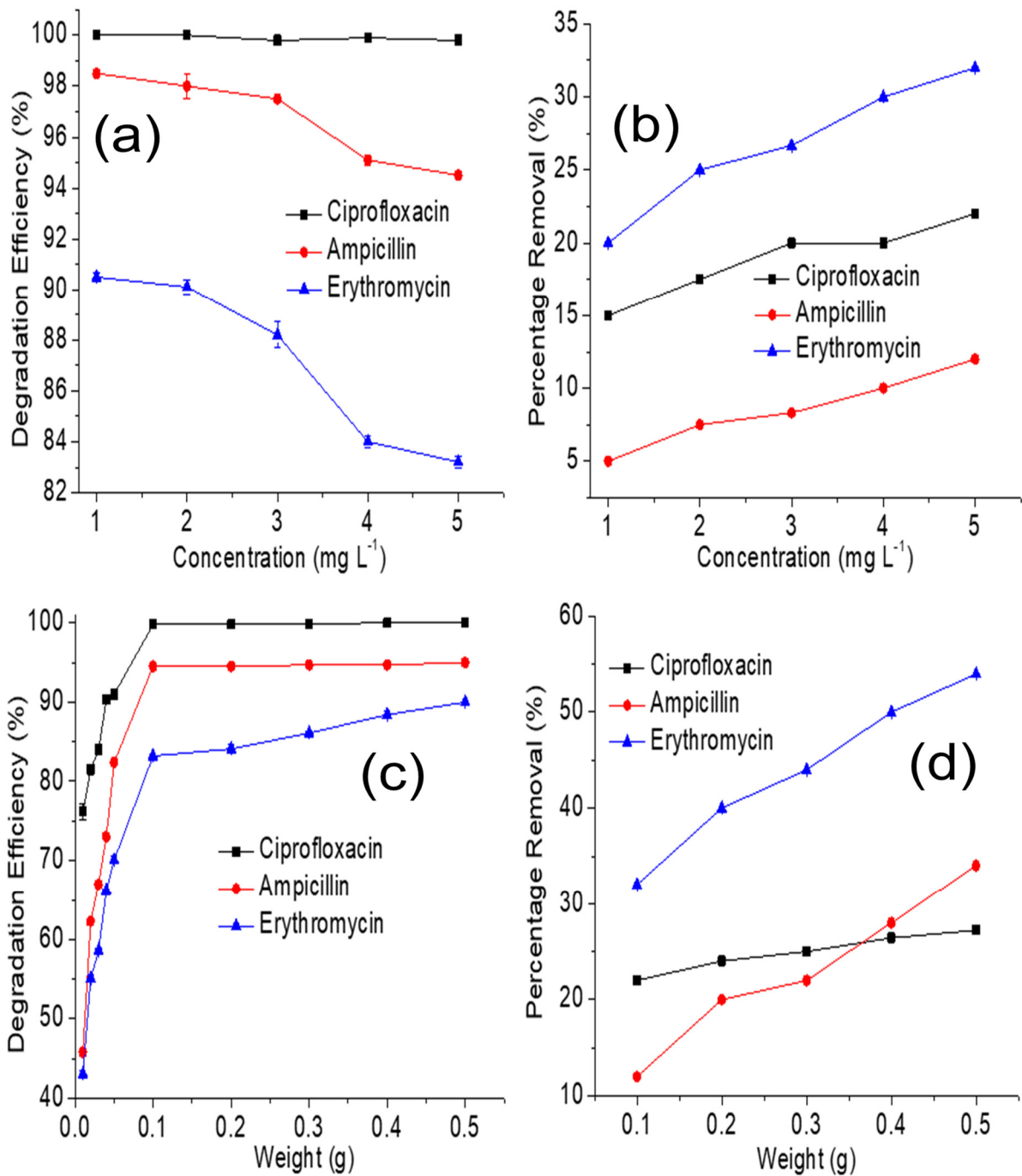
Figure 5. (**a**) = Effect of concentration of CIP, AMP and ERY on the degradation efficiency of ZnFe$_2$O$_4$@Chitosan, (**b**) = Effect of concentration of CIP, AMP and ERY on the percentage removal expressed by ZnFe$_2$O$_4$@Chitosan in the absence of visible light, (**c**) = Effect of weight of ZnFe$_2$O$_4$@Chitosan on degradation efficiency towards CIP, AMP and ERY at 5.00 mg L^{-1} and (**d**) = Effect of weight of ZnFe$_2$O$_4$@Chitosan on percentage removal expressed towards CIP, AMP and ERY at 5.00 mg L^{-1} in the absence of visible light.

The effect of weight of ZnFe$_2$O$_4$@Chitosan was also examined on the degradation efficiency and the percentage removal, as shown in Figure 5c,d. It was observed in both cases that the performance of ZnFe$_2$O$_4$@Chitosan towards the degradation of CIP, AMP and ERY increased as the weight of ZnFe$_2$O$_4$@Chitosan increased. This observation suggests that, as the weight of ZnFe$_2$O$_4$@Chitosan increased, more active sites were available to

initiate photodegradation and adsorption. Solution pH plays an important role in the photodegradation process.

ZnFe$_2$O$_4$@Chitosan expressed high degradation efficiency at low pH values but the degradation efficiency decreased as the pH increases above 7 (Figure 6a,b).
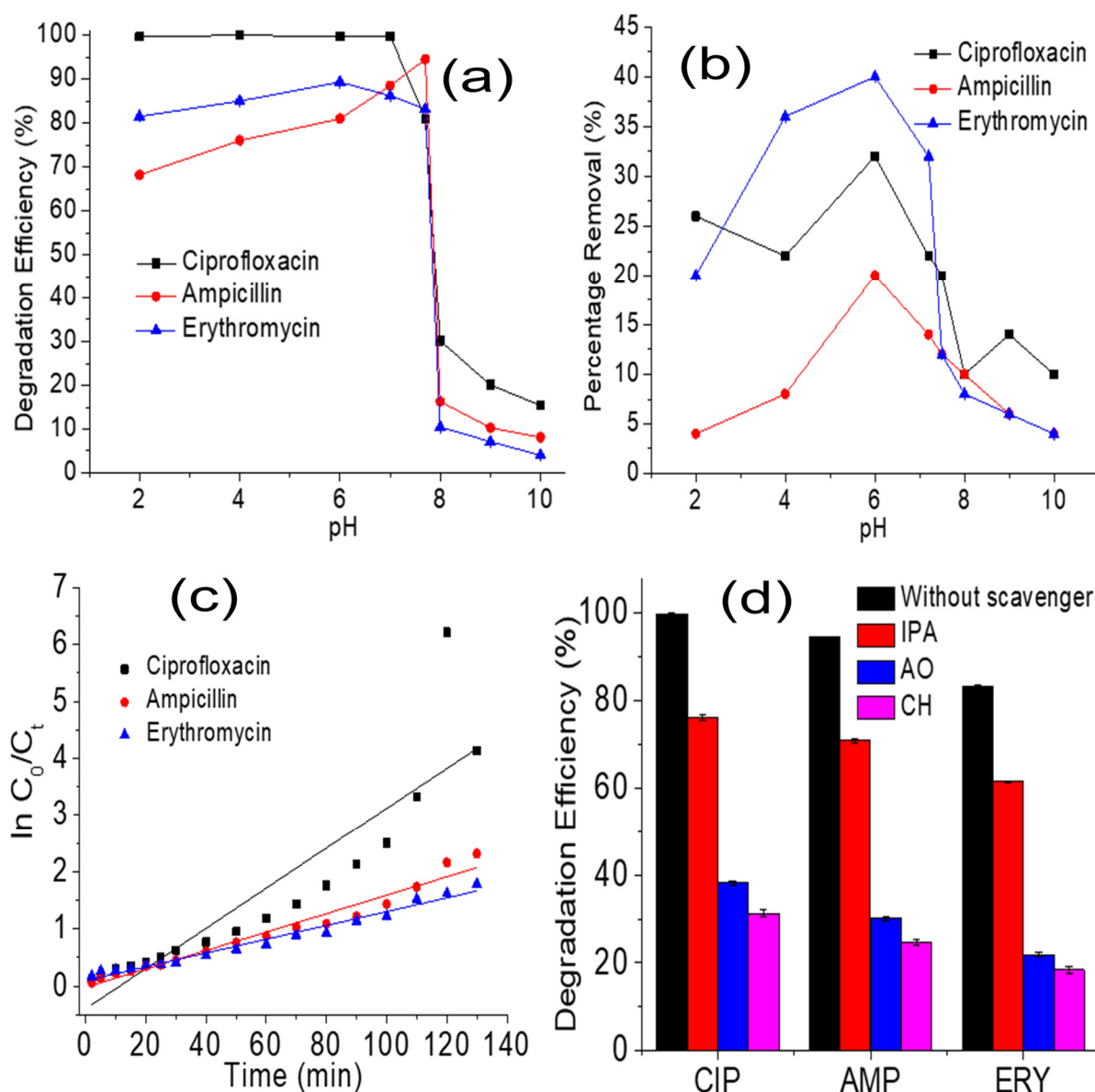

Figure 6. (**a**) = Effect of solution pH on the degradation efficiency of ZnFe$_2$O$_4$@Chitosan (0.1 g) against CIP, AMP and ERY at 5.00 mg L^{-1}, (**b**) = Effect of solution pH on the percentage removal expressed by ZnFe$_2$O$_4$@Chitosan (0.1 g) towards CIP, AMP and ERY at 5.00 mg L^{-1}, (**c**) = Plot of 1nCo/Ct versus irradiation time for CIP, AMP and ERY at 5.00 mg L^{-1} and 0.1 g of ZnFe$_2$O$_4$@Chitosan and (**d**) = Degradation efficiency of ZnFe$_2$O$_4$@Chitosan towards CIP, AMP and ERY with and without different ROS scavengers.

The best pH for the photodegradation study is the acidic pH, which may be due to the fact that during low pH, more H$^+$ ions are available that can react with water to form the hydroxyl radicals to promote the photodegradation process. On the other hand, the adsorption capacity was low at acidic pH (low pH value) but increased as the pH value increased towards 7 (neutral pH value). Interestingly, the percentage removal dropped as the pH value increased from 7 to 10.

The photodegradation of CIP, AMP and ERY by $ZnFe_2O_4$@Chitosan was subjected to a pseudo-first-order kinetic model, which can be described as:

$$In\left(\frac{C_o}{C_t}\right) = kt \tag{8}$$

where C_o and C_t are the initial and time "t" concentrations of CIP, AMP or ERY, respectively. The pseudo-first-order rate constant was calculated from the slope of the graph of $1nC_o/C_t$ versus time (Figure 6c) and represented as k, while t is the irradiation time. The pseudo-first-order rate constant for CIP is 0.035 min^{-1}, AMP is 0.016 min^{-1} and ERY is 0.012 min^{-1}. The values obtained for the pseudo-first-order rate constant is also reflective of the degradation efficiency exhibited by $ZnFe_2O_4$@Chitosan towards the antibiotics. The highest degradation efficiency was towards CIP (99.80 $\pm$ 0.20%), with the highest rate constant compared to other antibiotics. The higher the rate constant, the faster the process is expected with high degradation efficiency.

3.4. Proposed Mechanism for the Photodegradation of CIP, AMP and ERY by $ZnFe_2O_4$@Chitosan

Most photocatalytic degradation processes are known to be via reactive oxygen species (ROS) generation within the solution to be degraded. Therefore, the photocatalytic degradation exhibited by $ZnFe_2O_4$@Chitosan towards CIP, AMP and ERY was evaluated in the presence of IPA to scavenge hydroxyl radical (OH˙), AO to scavenge hole (h^+) and CH to scavenge superoxide ion radical ($\cdot O_2^-$), as previously reported [38]. The results obtained are presented in Figure 6d. It was observed that the photodegradation efficiency of $ZnFe_2O_4$@Chitosan was reduced in the presence of IPA, AO and CH, indicating that they all played roles in the degradation of CIP, AMP and ERY by $ZnFe_2O_4$@Chitosan. When CH was introduced into the degradation medium, there was a drastic reduction in the degradation efficiency from 99.80 $\pm$ 0.20% to 31.20 $\pm$ 0.80% in CIP, 94.50 $\pm$ 0.10% to 24.70 $\pm$ 0.50% in AMP and 83.20 $\pm$ 0.20% to 18.40 $\pm$ 0.70% in ERY. A similar observation also took place when AO was introduced into the medium, which suggested the scavenging of hole by AO and superoxide ion radicals by CH during the photodegradation process. This drastic reduction is an indication that both hole and superoxide ion radicals played an important role in the photodegradation process by $ZnFe_2O_4$@Chitosan.

Furthermore, the reduction in efficiency when IPA was introduced also confirmed that hydroxyl and superoxide ion radicals must have been generated from the photochemical reactions between the hole (h^+) and photoexcited electrons (e^-) with H_2O and O_2 molecules (Figure 7). As described in Figure 7a, during the process, $ZnFe_2O_4$@Chitosan may have absorbed visible-light energy greater than its bandgap, leading to the generation of h^+ in the valence band and e^- in the conduction band. As long as the recombination of h^+ and e^- is hindered, the ROS continues to promote the degradation of CIP, AMP or ERY, as described in Figure 7b.

3.5. Re-Useability and Stability of $ZnFe_2O_4$@Chitosan

The re-useability and stability of a photocatalyst plays an important role in determining its economic viability. In this regard, $ZnFe_2O_4$@Chitosan was regenerated using different solvent systems based on the solubility of CIP, AMP and ERY. Solvents used included deionized water, 0.1 M HCl, ethanol or a mixture of ethanol and 0.1 M HCl (3:2). However, a mixture of ethanol and 0.1 M HCl (3:2) gave better results in regenerating $ZnFe_2O_4$@Chitosan for re-use (Figure 8a). Therefore, at the end of each cycle, $ZnFe_2O_4$@Chitosan was washed with a mixture of ethanol and 0.1 M HCl (3:2), dried and re-used for the photodegradation of CIP, AMP or ERY. The cycle was repeated until the 15th cycle and the regeneration capacity for 15 successive cycles is shown in Figure 8b. Interestingly, the capacity was 97.60 $\pm$ 0.10% for CIP, 93.50 $\pm$ 0.20% for AMP and 95.00 $\pm$ 0.10% for ERY at the 15th cycle, which suggests a high stability of $ZnFe_2O_4$@Chitosan as a viable photocatalyst for the photodegradation of CIP, AMP and ERY. The ICP–OES results revealed 0.08 ppm of Fe and 0.05 ppm of Zn in the solution after the 15th cycle, which

suggests that the $ZnFe_2O_4$ particles leached into solution during the photodegradation process. However, the leached amount is within the permissible limits for Fe (0.10 ppm) and Zn (5.00 ppm) in drinking water. The results obtained in this study were also compared with a catalyst previously reported, as shown in Table 1. $ZnFe_2O_4$@Chitosan compared favourably with a previously reported photocatalyst for the degradation of CIP, AMP and ERY. Distinctly, $ZnFe_2O_4$@Chitosan exhibited an encouraging stability with capacity above 90%, even at the 15th regeneration cycle for re-use, which demonstrates the economic viability or advantage of $ZnFe_2O_4$@Chitosan over most recently reported photocatalysts it was compared with in the literature. The efficiency towards the degradation of CIP exhibited by $ZnFe_2O_4$@Chitosan is higher than values recently reported for $Cu_2O/MoS_2/rGO$ (Selvamani et al. 2021) and ZnO [39]. The use of $ZnFe_2O_4$@Chitosan for photodegradation was conducted in the visible-light regions, which shows that its use does not require an additional cost for a UV source, unlike in the case of some of the previous studies [40–42].
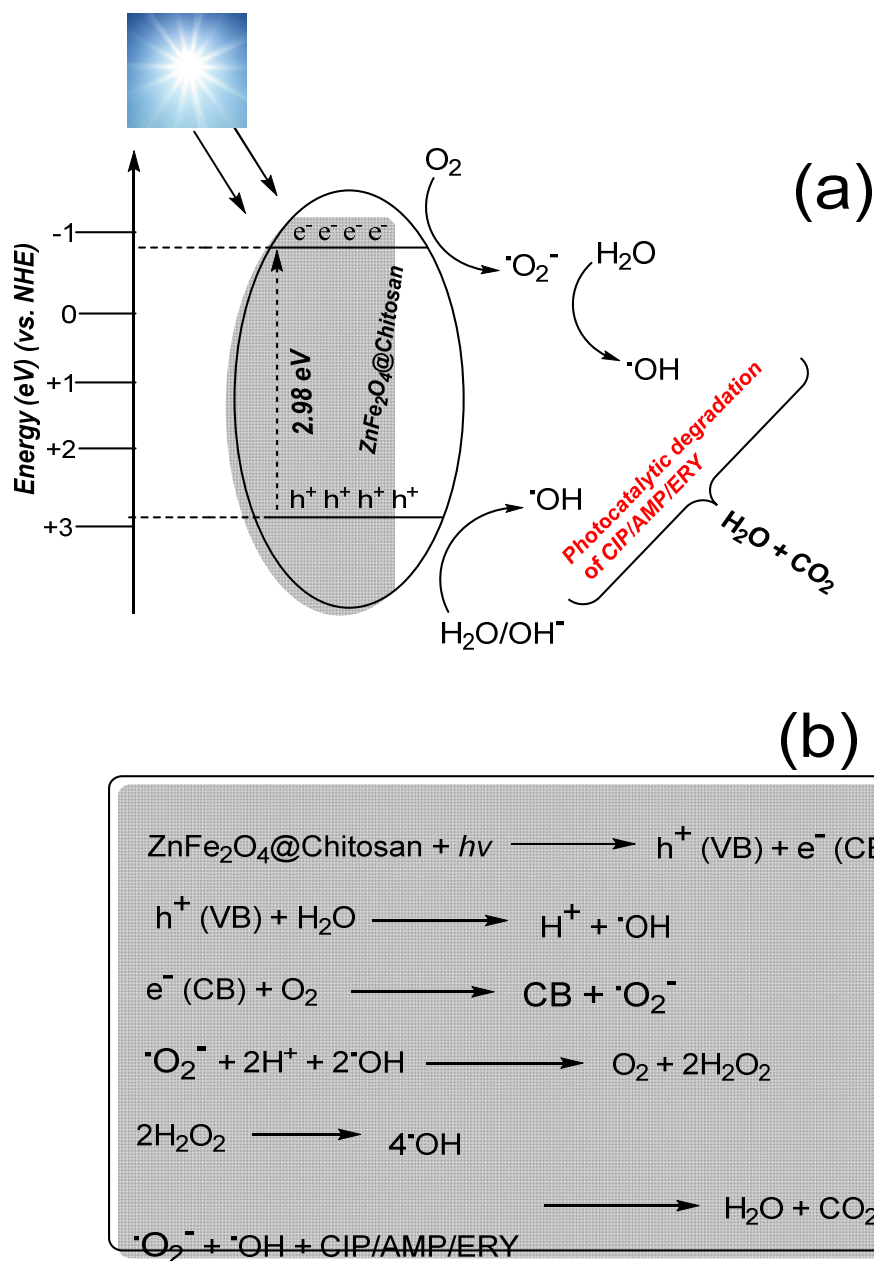

Figure 7. Proposed mechanism for the photodegradation of CIP, AMP and ERY: (**a**) Scheme for reaction mechanism and (**b**) Stepwise photodegradation of CIP, AMP and ERY.
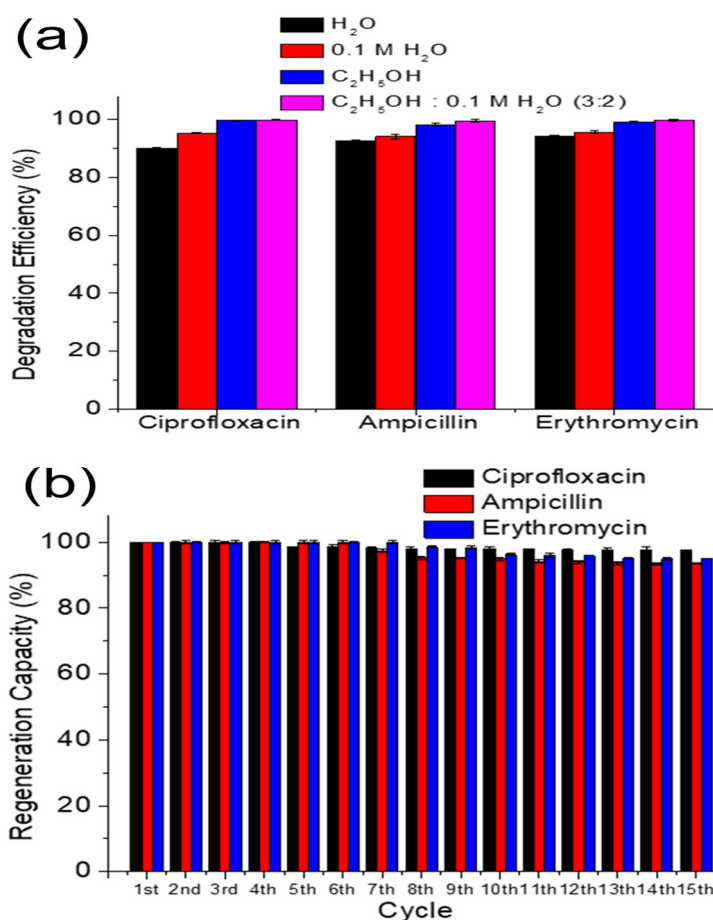
Figure 8. (**a**) Degradation efficiency of $ZnFe_2O_4$@Chitosan after washing with solvent systems and (**b**) Regeneration capacity of $ZnFe_2O_4$@Chitosan expressed towards CIP, AMP and ERY at different operational cycles.

Table 1. Comparison of the photodegradation of CIP, AMP and ERY by $ZnFe_2O_4$@Chitosan with other photocatalysts in literature.

Material	Antibiotic	DE (%)	LIS	AC (g L^{-1})	Conc (mg L^{-1})	Stability (%)	Reference
Cu_2O/MoS_2/rGO	CIP	55.00	150 W halogen lamp	0.30	10.00	-	[43]
TiO_2 on glass	CIP	92.00	6 W UV-C lamp	1.00	5.00	-	[44]
ZnO	CIP	93.00	8 W Hg fluorescent	0.50	5.00	-	[39]
ZnO	CIP	100.00	9 W Hg UV lamp	0.15	10.00	-	[42]
MWCNTs-$CuNiFe_2O_4$	AMP	100.00	36 W UV	0.50	25.00	93.72 (8th cycle)	[40]
$Ru/WO_3/ZrO_2$	AMP	96.00	150 W Xe lamp	1.00	50.00	92.00 (2nd cycle)	[41]
La/Cu/Zr trimetallic	AMP	86.00	Sunlight	0.10	50.00	59.00 (6th cycle)	[45]
Znpc–TiO_2	ERY	74.21	300 W Xe arc lamp	0.40	1×10^5 M	-	[46]
γ-Fe_2O_3/SiO_2	ERY	87.17	15 W UV-C lamp	0.50	6.00	-	[47]
Ag-NP	AMP	96.50	Sunlight	0.17	10.00	-	[48]
FeSi@MN	AMP	70.00	Sunlight	0.60	100.00	63.00 (4th cycle)	[49]
WO3/BiOCl/Chitosan	AMP	75.00	Solar light	0.50	* 1×10^{-4}	67.00 (10th cycle)	[50]
BiOCl/Chitosan	AMP	75.00	Solar light	1.00	* 1×10^{-4}	67.00 (10th cycle)	[51]
Fe^{III}-CS-GLA	CIP	90.30	Solar light	-	** 50	-	[52]
$ZnFe_2O_4$@Chitosan	CIP	99.80	Visible-light	1.00	5.00	97.60 (15th cycle)	This study
	AMP	94.50	simulation (150 W	1.00	5.00	93.50 (15th cycle)	
	ERY	83.20	Xe light)	1.00	5.00	95.00 (15th cycle)	

- = Not reported. Degradation efficiency = DE, Light illumination source = LIS, Amount of catalyst = AC, Conc = Concentration of antibiotic, Nickel-copper ferrite nanoparticles onto multi-walled carbon nanotubes = MWCNTs-$CuNiFe_2O_4$, FeSi@magnetic nanoparticle = FeSi@MN, Ciprofloxacin = CIP, Ampicillin = AMP, Erythromycin = ERY, * = mol dm^{-3}, Fe^{III}-CS-GLA = iron (III) chelated cross-linked chitosan, ** = μM.

4. Conclusions

ZnFe$_2$O$_4$@Chitosan was prepared by simple chemical process and applied in the photodegradation of CIP, AMP and ERY in aqueous solution. The results from the FTIR of ZnFe$_2$O$_4$@Chitosan revealed prominent peaks, suggesting its synthesis, while signals from XRD showed a diffraction pattern confirming the synthesis of ZnFe$_2$O$_4$@Chitosan with a crystallite size of 35.14 nm. The VSM result revealed a saturation magnetization of 2.38 emu g^{-1}, which is large enough for magnetic separation for practical applications. The study showed that both photodegradation and adsorption were taking place at the same time with the percentage degradation efficiency in the order CIP (99.80 $\pm$ 0.20%) > AMP (94.50 $\pm$ 0.10%) > ERY (83.20 $\pm$ 0.20%). ZnFe$_2$O$_4$@Chitosan exhibited an encouraging stability with capacity above 90%, even at the 15th regeneration cycle. The photodegradation mechanism suggested the role of hydroxyl and superoxide ion radicals. The study revealed ZnFe$_2$O$_4$@Chitosan to be a promising catalyst for the degradation of CIP, AMP and ERY in aqueous solution.

Author Contributions: Formal analysis: N.A.H.M., A.A., R.N.S. Investigations: N.A.H.M., A.A., R.N.S. Methodology: N.A.H.M., A.A., R.N.S., S.E. Software: N.A.H.M., R.N.S. Resources: N.A.H.M., A.A., R.N.S. Supervision: A.A., R.N.S., S.E. Writing—original draft: A.A. Writing—review& editing: N.A.H.M., A.A., R.N.S., S.E. All authors have read and agreed to the published version of the manuscript.

References

1. Hanna, N.; Sun, P.; Sun, Q.; Li, X.; Yang, X.; Ji, X.; Zou, H.; Ottoson, J.; Nilsson, L.E.; Berglund, B.; et al. Presence of antibiotic residues in various environmental compartments of Shandong province in eastern China: Its potential for resistance development and ecological and human risk. *Environ. Int.* **2018**, *114*, 131–142. [CrossRef] [PubMed]
2. Zalewska, M.; Błażejewska, A.; Czapko, A.; Popowska, M. Antibiotics and Antibiotic Resistance Genes in Animal Manure– Consequences of Its Application in Agriculture. *Front. Microbiol.* **2021**, *12*, 610656. [CrossRef] [PubMed]
3. Kumar, M.; Jaiswal, S.; Sodhi, K.K.; Shree, P.; Singh, D.K.; Agrawal, P.K.; Shukla, P. Antibiotics bioremediation: Perspectives on its ecotoxicity and resistance. *Environ. Int.* **2019**, *124*, 448–461. [CrossRef] [PubMed]
4. Lv, J.; Zhang, L.; Chen, Y.; Ye, B.; Han, J.; Jin, N. Occurrence and distribution of pharmaceuticals in raw, finished, and drinking water from seven large river basins in China. *J. Water Health* **2019**, *17*, 477–489. [CrossRef]
5. Lyu, J.; Chen, Y.; Zhang, L. Antibiotics in Drinking Water and Health Risks—China, 2017. *China CDC Wkly.* **2020**, *2*, 413–417. [CrossRef]
6. Azanu, D.; Styrishave, B.; Darko, G.; Weisser, J.J.; Abaidoo, R.C. Occurrence and risk assessment of antibiotics in water and lettuce in Ghana. *Sci. Total Environ.* **2018**, *622–623*, 293–305. [CrossRef]
7. Guruge, K.S.; Goswami, P.; Tanoue, R.; Nomiyama, K.; Wijesekara, R.; Dharmaratne, T.S. First nationwide investigation and environmental risk assessment of 72 pharmaceuticals and personal care products from Sri Lankan surface waterways. *Sci. Total Environ.* **2019**, *690*, 683–695. [CrossRef]
8. Lorenzo, P.; Adriana, A.; Jessica, S.; Carles, B.; Marinella, F.; Marta, L.; Luis, B.J.; Pierre, S. Antibiotic resistance in urban and hospital wastewaters and their impact on a receiving freshwater ecosystem. *Chemosphere* **2018**, *206*, 70–82. [CrossRef]
9. Tran, N.H.; Hoang, L.; Nghiem, L.D.; Nguyen, N.M.H.; Ngo, H.H.; Guo, W.; Trinh, Q.T.; Mai, N.H.; Chen, H.; Nguyen, D.D.; et al. Occurrence and risk assessment of multiple classes of antibiotics in urban canals and lakes in Hanoi, Vietnam. *Sci. Total Environ.* **2019**, *692*, 157–174. [CrossRef]
10. Gholami, P.; Khataee, A.; Soltani, R.D.C.; Dinpazhoh, L.; Bhatnagar, A. Photocatalytic degradation of gemifloxacin antibiotic using Zn-Co-LDH@biochar nanocomposite. *J. Hazard. Mater.* **2020**, *382*, 121070. [CrossRef]
11. Khaledian, H.R.; Zolfaghari, P.; Elhami, V.; Aghbolaghy, M.; Khorram, S.; Karimi, A.; Khataee, A. Modification of immobilized titanium dioxide nanostructures by argon plasma for photocatalytic removal of organic dyes. *Molecules* **2019**, *24*, 383. [CrossRef]

12. Zhang, S.; Khan, I.; Qin, X.; Qi, K.; Liu, Y.; Bai, S. Construction of 1D Ag-AgBr/AlOOH plasmonic photocatalyst for degradation of tetracycline hydrochloride. *Front. Chem.* **2020**, *8*, 117. [CrossRef]

13. Yang, X.; Chen, Z.; Zhao, W.; Liu, C.; Qian, X.; Zhang, M.; Wei, G.; Khan, E.; Ng, Y.H.; Ok, Y.S. Recent advances in photodegradation of antibiotic residues in water. *Chem. Eng. J.* **2021**, *405*, 126806. [CrossRef]

14. Elmolla, E.S.; Chaudhuri, M. Degradation of amoxicillin, ampicillin and cloxacillin antibiotics in aqueous solution by the UV/ZnO photocatalytic process. *J. Hazard. Mater.* **2010**, *173*, 445–449. [CrossRef]

15. Amariei, G.; Valenzuela, L.; Iglesias-Juez, A.; Rosal, R.; Visa, M. ZnO-functionalized fly-ash based zeolite for ciprofloxacin antibiotic degradation and pathogen inactivation. *J. Environ. Chem. Eng.* **2022**, *10*, 107603. [CrossRef]

16. Mishra, S.; Kumar, P.; Samanta, S.K. Microwave Catalytic Degradation of Antibiotic Molecules by 2D Sheets of Spinel Nickel Ferrite. *Ind. Eng. Chem. Res.* **2020**, *59*, 15839–15847. [CrossRef]

17. Becker, A.; Kirchberg, K.; Marschall, R. Magnesium ferrite ($MgFe_2O_4$) nanoparticles for photocatalytic antibiotics degradation. *Z. Phys. Chem.* **2020**, *234*, 645–654. [CrossRef]

18. Li, Y.; He, J.; Zhang, K.; Hong, P.; Wang, C.; Kong, L.; Liu, J. Oxidative degradation of sulfamethoxazole antibiotic catalyzed by porous magnetic manganese ferrite nanoparticles: Mechanism and by-products identification. *J. Mater. Sci.* **2020**, *55*, 13767–13784. [CrossRef]

19. Yi, H.; Lai, C.; Almatrafi, E.; Huo, X.; Qin, L.; Fu, Y.; Zhou, C.; Zeng, Z.; Zeng, G. Efficient antibiotics removal via the synergistic effect of manganese ferrite and MoS_2. *Chemosphere* **2022**, *288*, 132494. [CrossRef]

20. Zhong, Y.; Shih, K.; Diao, Z.; Song, G.; Su, M.; Hou, L.; Chen, D.; Kong, L. Peroxymonosulfate activation through LED-induced $ZnFe_2O_4$ for levofloxacin degradation. *Chem. Eng. J.* **2021**, *417*, 129225. [CrossRef]

21. Senapati, K.K.; Roy, S.; Borgohain, C.; Phukan, P. Palladium nanoparticle supported on cobalt ferrite: An efficient magnetically separable catalyst for ligand free Suzuki coupling. *J. Mol. Catal. A Chem.* **2012**, *352*, 128–134. [CrossRef]

22. Yao, C.; Zeng, Q.; Goya, G.; Torres, T.; Liu, J.; Wu, H.; Ge, M.; Zeng, Y.; Wang, Y.; Jiang, J. $ZnFe_2O_4$ nanocrystals: Synthesis and magnetic properties. *J. Phys. Chem. C* **2007**, *111*, 12274–12278. [CrossRef]

23. Abbasian, A.R.; Afarani, M.S. One-step solution combustion synthesis and characterization of $ZnFe_2O_4$ and $ZnFe_{1.6}O_4$ nanoparticles. *Appl. Phys. A* **2019**, *125*, 721. [CrossRef]

24. Hammond, C. *The Basics of Crystallography and Diffraction*; Oxford University Press: New York, NY, USA, 1997.

25. Gherca, D.; Pui, A.; Cornei, N.; Cojocariu, A.; Nica, V.; Caltun, O. Synthesis, characterization and magnetic properties of MFe_2O_4 (M=Co, Mg, Mn, Ni) nanoparticles using ricin oil as capping agent. *J. Magn. Magn. Mater.* **2012**, *324*, 3906–3911. [CrossRef]

26. Bell, A.T. The impact of nanoscience on heterogeneous catalysis. *Science* **2013**, *299*, 1688–1691. [CrossRef]

27. Shang, M.; Wang, W.; Sun, S.; Zhou, L.; Zhang, L. Bi2WO6 nanocrystals with high photocatalytic activities under visible light. *The J. Phys. Chem. C* **2008**, *112*, 10407–10411. [CrossRef]

28. Hagfeldt, A.; Graetzel, M. Light-induced redox reactions in nanocrystalline systems. *Chem. Rev.* **1995**, *95*, 49–68. [CrossRef]

29. Nadeem, K.; Shahid, M.; Mumtaz, M. Competing crystallite size and zinc concentration in silica coated cobalt ferrite nanoparticles. *Prog. Nat. Sci. Mat. Intern.* **2014**, *24*, 199–204. [CrossRef]

30. Corazzari, I.; Nisticò, R.; Turci, F.; Faga, M.G.; Franzoso, F.; Tabasso, S.; Magnacca, G. Advanced physico-chemical characterization of chitosan by means of TGA coupled on-line with FTIR and GCMS: Thermal degradation and water adsorption capacity. *Polym. Degrad. Stab.* **2015**, *112*, 1–9. [CrossRef]

31. De Britto, D.; Campana-Filho, S.P. Kinetics of the thermal degradation of chitosan. *Thermochim. Acta* **2007**, *465*, 73–82. [CrossRef]

32. Avetta, P.; Nisticò, R.; Faga, M.G.; D'Angelo, D.; Boot, E.A.; Lamberti, R.; Martorana, S.; Calza, P.; Fabbri, D.; Magnacca, G. Hernia-repair prosthetic devices functionalised with chitosan and ciprofloxacin coating: Controlled release and antibacterial activity. *J. Mater. Chem. B* **2014**, *2*, 5287–5294. [CrossRef]

33. Hilding, J.; Grulke, E.A.; Sinnott, S.B.; Qian, D.; Andrews, R.; Jagtoyen, M. Sorption of Butane on Carbon Multiwall Nanotubes at Room Temperature. *Langmuir* **2001**, *17*, 7540–7544. [CrossRef]

34. De Britto, D.; Campana-Filho, S.P. A kinetic study on the thermal degradation of N,N,N-trimethylchitosan. *Polym. Degrad. Stab.* **2004**, *84*, 353–361. [CrossRef]

35. Zeng, L.; Qin, C.; Wang, L.; Li, W. Volatile compounds formed from the pyrolysis of chitosan. *Carbohydr. Polym.* **2011**, *83*, 1553–1557. [CrossRef]

36. Xu, Y.; Wu, S.; Li, X.; Huang, Y.; Wang, Z.; Han, Y.; Wu, J.; Meng, H.; Zhang, X. Synthesis, characterization, and photocatalytic degradation properties of ZnO/$ZnFe_2O_4$ magnetic heterostructures. *New J. Chem.* **2017**, *41*, 15433–15438. [CrossRef]

37. Xue, H.; Li, Z.; Wang, X.; Fu, X. Facile synthesis of nanocrystalline zinc ferrite via a self-propagating combustion method. *Mater. Lett.* **2007**, *61*, 347–350. [CrossRef]

38. Sharma, A.; Dutta, R.K. Se-doped CuO NPs/H_2O_2/UV as a highly efficient and sustainable photo-Fenton catalytic system for enhanced degradation of 4-bromophenol. *J. Clean. Prod.* **2018**, *185*, 464–475. [CrossRef]

39. Ulyankina, A.; Molodtsova, T.; Gorshenkov, M.; Leontyev, I.; Zhigunov, D.; Konstantinova, E.; Lastovina, T.; Tolasz, J.; Henych, J.; Licciardello, N.; et al. Photocatalytic degradation of ciprofloxacin in water at nano-ZnO prepared by pulse alternating current electrochemical synthesis. *J. Water Process Eng.* **2021**, *40*, 101809. [CrossRef]

40. Al-Musawi, T.J.; Rajiv, P.; Mengelizadeh, N.; Arghavan, F.S.; Balarak, D. Photocatalytic efficiency of $CuNiFe_2O_4$ nanoparticles loaded on multi-walled carbon nanotubes as a novel photocatalyst for ampicillin degradation. *J. Mol. Liq.* **2021**, *337*, 116470. [CrossRef]

41. Alalm, M.G.; Ookawara, S.; Fukushi, D.; Sato, A.; Tawfik, A. Improved WO_3 photocatalytic efficiency using ZrO_2 and Ru for the degradation of carbofuran and ampicillin. *J. Hazard. Mater.* **2016**, *302*, 225–231. [CrossRef]

42. Eskandari, M.; Goudarzi, N.; Moussavi, G. Application of low-voltage UVC light and synthetic ZnO nanoparticles to photocatalytic degradation of ciprofloxacin in aqueous sample solutions. *Water Environ. J.* **2018**, *32*, 58–66. [CrossRef]

43. Selvamani, P.S.; Vijaya, J.J.; Kennedy, L.J.; Mustafa, A.; Bououdina, M.; Sophia, P.J.; Ramalingam, R.J. Synergic effect of $Cu_2O/MoS_2/rGO$ for the sonophotocatalytic degradation of tetracycline and ciprofloxacin antibiotics. *Ceram. Int.* **2021**, *47*, 4226–4237. [CrossRef]

44. Malakootian, M.; Nasiri, A.; Amiri Gharaghani, M. Photocatalytic degradation of ciprofloxacin antibiotic by TiO_2 nanoparticles immobilized on a glass plate. *Chem. Eng. Commun.* **2020**, *207*, 56–72. [CrossRef]

45. Sharma, G.; Gupta, V.K.; Agarwal, S.; Bhogal, S.; Naushad, M.; Kumar, A.; Stadler, F.J. Fabrication and characterization of trimetallic nano-photocatalyst for remediation of ampicillin antibiotic. *J. Mol. Liq.* **2018**, *260*, 342–350. [CrossRef]

46. Vignesh, K.; Rajarajan, M.; Suganthi, A. Photocatalytic degradation of erythromycin under visible light by zinc phthalocyanine-modified titania nanoparticles. *Mater. Sci. Semicond. Process.* **2014**, *23*, 98–103. [CrossRef]

47. Fakhri, A.; Rashidi, S.; Tyagi, I.; Agarwal, S.; Gupta, V.K. Photodegradation of Erythromycin antibiotic by γ-Fe_2O_3/SiO_2 nanocomposite: Response surface methodology modeling and optimization. *J. Mol. Liq.* **2016**, *214*, 378–383. [CrossRef]

48. Jassal, P.; Khajuria, R.; Sharma, R.; Debnath, P.; Verma, S.; Johnson, A.; Kumar, S. Photocatalytic degradation of ampicillin using silver nanoparticles biosynthesised by *Pleurotus ostreatus*. *BioTechnologia* **2020**, *101*, 5–14. [CrossRef]

49. Sohrabnezhad, S.; Pourahmad, A.; Karimi, M.F. Magnetite-metal organic framework core@shell for degradation of ampicillin antibiotic in aqueous solution. *J. Solid State Chem.* **2020**, *288*, 121420. [CrossRef]

50. Singh, P.; Priya, B.; Shandilya, P.; Raizada, P.; Singh, N.; Pare, B.; Jonnalagadda, S. Photocatalytic mineralization of antibiotics using 60% WO3/BiOCl stacked to graphene sand composite and chitosan. *Arabian J. Chem.* **2019**, *12*, 4627–4645. [CrossRef]

51. Priya, B.; Shandilya, P.; Raizada, P.; Thakur, P.; Singh, N.; Singh, P. Photocatalytic mineralization and degradation kinetics of ampicillin and oxytetracycline antibiotics using graphene sand composite and chitosan supported BiOCl. *J. Molecul. Catal. A Chem.* **2016**, *423*, 400–413. [CrossRef]

52. Saha, S.; Saha, T.K.; Karmaker, S.; Islam, Z.; Demeshko, S.; Frauendorf, H.; Meyer, F. Solar Light-Assisted Oxidative Degradation of Ciprofloxacin in Aqueous Solution by Iron (III) Chelated Cross-Linked Chitosan Immobilized on a Glass Plate. *Catalysts* **2022**, *12*, 475. [CrossRef]